

# An NFC-CPT-Combined Coupler With Series-None Compensation for Metal-Cover Smartphone Applications

Jia-Qi Zhu, Yong-Ling Ban<sup>ID</sup>, Rui-Min Xu, *Member, IEEE*,  
and Chunting Chris Mi<sup>ID</sup>, *Fellow, IEEE*

**Abstract**—A near-field communication capacitive power transfer (NFC-CPT)-combined coupler with a series-none compensation topology is proposed for metal-cover smartphone applications. To achieve capacitive power transfer through metal cover, the metal cover itself is used as the receiving metal plates. To realize NFC through metal cover, the cross slot including a slim horizontal slot and a rectangular slot is embedded on the metal cover, which mitigates the eddy current loss and increases the inductive coupling for the NFC antenna. Besides, the cross slot divides the metal cover into two separate metal plates, which is necessary for capacitive power transfer. Considering the space limitation and safety requirement, no compensation components are integrated inside the smartphone and only a series inductance is integrated on the transmitter side. A prototype of the proposed NFC-CPT-combined coupler has been built. The wireless power transfer and NFC through metal cover have been validated through experiment. The experimental results show that the prototype achieves 5-W output power with a 93.5% circuit efficiency at 6.78 MHz, and the detection range of the NFC antenna is 61 mm.

**Index Terms**—Capacitive power transfer, metal cover, near-field communication (NFC), smartphone application, series-none (SN).

## I. INTRODUCTION

**I**NDUCTIVE power transfer (IPT) and capacitive power transfer (CPT) are two primary technologies for wireless power transfer (WPT), using magnetic field and electric field as media, respectively [1]–[3]. IPT is widely applied for wireless charging of portable devices using the Qi standard [4]. However, for a metal-cover smartphone, the metal cover will

become a metal barrier between the transmitting coil and the receiving coil and eddy current will be induced, resulting in a low efficiency [5], [6]. In addition, ferrite materials are usually required in an IPT system to enhance magnetic coupling and aluminum plates are used for shielding, leading to an increase in thickness and weight of the charging system, which is not suitable for compact smartphone applications. In this case, CPT is a good alternative for consumer electronic devices such as metal-cover smartphone applications [7]–[9]. High-frequency electric field is used to transfer power through the metal cover without significant power losses (eddy current). Thin metal plates can be adopted to meet the compact requirement of smartphone applications and save cost.

As indicated in [10], a double-sided LCLC-compensated topology was proposed to achieve CPT for a 2.4-kW CPT system. In [11], a four-plate capacitive coupler was proposed with the LCLC-compensated topology. The vertical layout of the capacitive plates helped save space and compensation capacitors. As reported in [12], a double-sided LC-compensation topology was proposed for a loosely coupled CPT system. A CPT platform with soft switched transformer control was investigated in [13]. By energizing specific individual primary charging plates and varying the compensation inductance, a free-positioning CPT was realized. A capacitive coupler array with free-positioning features for mobile tablet applications was studied in [14]. Only two fixed compensation inductances were implemented at the transmitter and receiver sides to achieve a free-positioning CPT. In the above CPT schemes, the primary and secondary capacitive plates are all made up of regular rectangular metal plates. The metal plates with big planar sizes occupy a lot of space but do not benefit other applications of the system. In fact, with similar overall planar size and distance among the metal plates, the shape of the metal plates can be varied and optimized to work for other applications without performance degradation in CPT. This feature of CPT is good for compact consumer electronic systems, such as smartphone applications. By taking advantage of this feature of CPT, this article proposes a combined coupler for metal-cover smartphone applications.

Near-field communication (NFC) is a contactless technology that operates at 13.56 MHz within close proximity [15]. With the leading trend of building near-cashless society in many countries, NFC has become a prerequisite part of nowadays smartphones. Integrating an NFC antenna into a

Manuscript received December 17, 2019; revised March 13, 2020 and May 13, 2020; accepted May 29, 2020. Date of publication June 16, 2020; date of current version May 28, 2021. This work was supported in part by the National Natural Science Foundation of China under Grant 61471098, in part by the National Higher-education Institution General Research and Development Project under Grant ZYGX2016J035 and Grant ZYGX2018J037, and in part by the China Scholarship Council. Recommended for publication by Associate Editor Chi K. Lee. (*Corresponding authors: Yong-Ling Ban; Chunting Chris Mi.*)

Jia-Qi Zhu is with the School of Electronic Engineering, University of Electronic Science and Technology of China, Chengdu 611731, China, and also with the Department of Electrical and Computer Engineering, San Diego State University, San Diego, CA 92182 USA (e-mail: jia-qi.zhu@foxmail.com).

Yong-Ling Ban and Rui-Min Xu are with the School of Electronic Engineering, University of Electronic Science and Technology of China, Chengdu 611731, China (e-mail: byl@uestc.edu.cn; rmxu@uestc.edu.cn).

Chunting Chris Mi is with the Department of Electrical and Computer Engineering, San Diego State University, San Diego, CA 92182 USA (e-mail: mi@ieee.org).

Color versions of one or more of the figures in this article are available online at <https://ieeexplore.ieee.org>.

Digital Object Identifier 10.1109/JESTPE.2020.3002858

smartphone with nonmetallic case is already a developed technology [16]–[18]. However, with a metallic case sandwiched between the NFC antenna and the transponder, eddy current will be induced on the surfaces of the metal cover and the magnetic field lines will be blocked [19]. With the advantage of aesthetic appearance and robust mechanical strength of a metal cover, embedding NFC antenna into a metal-cover smartphone is a significant research area.

To reduce the eddy current loss in a metal cover, several techniques were investigated [20]–[25]. As indicated by Nakano [20], a main horizontal slot and a square slot together with an additional vertical slot were implemented on the metal cover to change the induced eddy current distribution, thus mitigating eddy current losses. By placing an irregular and nonmeandering dual-loop NFC antenna coil at the center of a rectangular slot, the direction of the eddy current induced on the metal cover will become the same as the current flowing on the NFC antenna coil [23]. As reported in [25], by properly integrating a series capacitor at the end of the main horizontal slot and tuning the compensation circuit of the NFC antenna, the metal cover was transformed from a negative gain to a booster for the NFC antenna, resulting in a better performance than a sole NFC antenna in free-space condition. Above all, either an additional vertical slot [20], [21] or an irregular NFC antenna coil [22]–[24] is needed to achieve NFC for metal-cover smartphones. The additional vertical slot will bring down the aesthetic appearance and break down the mechanical strength of the metal cover. The traces of the irregular NFC antenna coil need to be wound through the rectangular slot or between the two rectangular slots. In real industrial applications, the rectangular slot normally represents a camera hole or a fingerprint hole. Because the space beneath or between these holes is very limited, it is hard for the NFC antenna coil to be placed in this space.

In this article, an NFC-CPT-combined coupler with series-*non* (SN) compensation topology for metal-cover smartphone applications is proposed. To achieve NFC through metal-cover block, a 2-mm slot and a rectangular slot (cross slot) are loaded on the metal cover, which alters the current distribution on the metal cover and thus reducing the eddy current loss for the NFC antenna. Unlike [21]–[24], the NFC antenna coil is wound around the rectangular slot, which is more reasonable and applicable in real industrial applications. With the cross slot, the metal cover is divided into two separate metal plates. These two metal plates serve as the receiving capacitive plates so that no metallic components exist between the transmitting plates and the receiving plates. CPT for a metal-cover smartphone is thus achieved. Moreover, unlike conventional CPT system with regular rectangular metal plates [10]–[14], the capacitive couplers in this article are optimized to change the eddy current distribution on the metal cover and thus mitigating the eddy current loss for the NFC antenna. Different from the double-sided LCLC topology in [10], the double-sided LCL topology in [11], and the double-sided LC topology in [12], an SN compensation topology for CPT is proposed in this article to reach safety voltage range on the metal cover and save internal space for metal-cover smartphones. Above all, the advantages of the proposed combined coupler can be

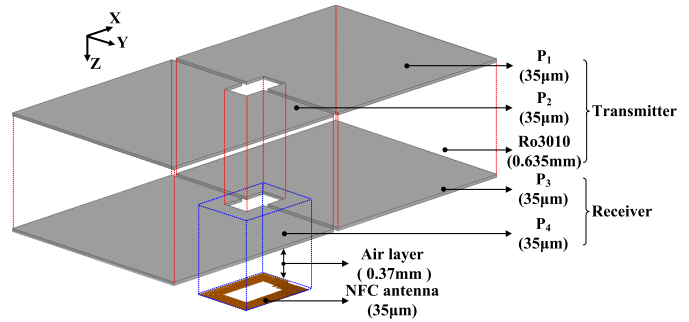


Fig. 1. Side view of the proposed NFC-CPT-combined coupler.

summarized as below. First, WPT is achieved through metal cover without eddy current loss. Because metal cover itself is used as the receiving plates, the space and cost of the smartphone are saved. Second, the size and shape of the metal cover are optimized to realize NFC through metal cover and they benefit each other. Third, an SN compensation topology is proposed so that none compensation component is embedded inside the smartphone, leading to space and cost reduction.

## II. STRUCTURE OF THE NFC-CPT-COMBINED COUPLER

The side view of the proposed NFC-CPT-combined coupler for smartphone is shown in Fig. 1. On the top of the stack are two irregular metal plates, that is,  $P_1$  and  $P_2$ , which construct the transmitting plates of the CPT system. A Ro3010 substrate ( $\epsilon_r = 10.2$ ) of 0.635 mm is sandwiched between the transmitting plates ( $P_1$ ,  $P_2$ ) and the receiving plates ( $P_3$ ,  $P_4$ ), leading to high coupling capacitance. The metal cover is composed of receiving coupling plates  $P_3$  and  $P_4$ , whose shape and dimension are the same as  $P_1$  and  $P_2$ . At the bottom of the stack is the NFC antenna coil, which is attached to  $P_3$  and  $P_4$  through an adhesive layer of 0.37-mm thickness. Here, the transmitter is composed of the transmitting plates ( $P_1$ ,  $P_2$ ) and the Ro3010 dielectric layer, while the receiving plates (metal cover of  $P_3$ ,  $P_4$ ) and the NFC antenna construct the receiver inside the smartphone. During wireless charging process, the smartphone is supposed to be placed on the transmitter so that the transmission distance of the proposed coupler is 0.635 mm.

The plan view of the NFC-CPT-combined coupler for a smartphone is shown in Fig. 2(a). An 18 mm  $\times$  10 mm rectangular slot together with a 2-mm-width horizontal slot are located at the center of the metal cover, separating the metal cover into two identical metal plates, namely,  $P_3$  and  $P_4$ . Under the two metal plates, a regular miniaturized NFC antenna coil winds around the rectangular slot. As shown in Fig. 2(b), the planar size of the NFC antenna coil is 30 mm  $\times$  22 mm with a line width  $W$  of 0.8 mm and line gap  $G$  of 0.4 mm. Here, the feed port is located at the top of the NFC antenna, where a jumper line is linked to one of its feed lines from the midtop.

## III. ANALYSIS OF THE NFC ANTENNA

### A. Design of the NFC Antenna Coil

ANSYS HFSS is used to analyze the NFC antenna in this section. For compact consideration, the planar size of the NFC antenna coil is set as 30 mm  $\times$  22 mm. With the

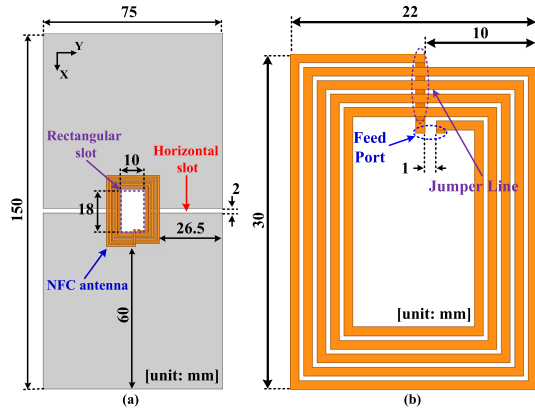


Fig. 2. Plan view of the (a) NFC-CPT-combined coupler and (b) sole NFC antenna coil.

TABLE I

SIMULATED PARAMETERS OF THE PROPOSED NFC ANTENNA REGARDING LINE WIDTH AND LINE GAP

| Parameter               | $W=0.5$ mm | $W=0.6$ mm | $W=0.7$ mm | $W=0.8$ mm |
|-------------------------|------------|------------|------------|------------|
|                         | $G=0.1$ mm | $G=0.2$ mm | $G=0.3$ mm | $G=0.4$ mm |
| $L_a$ [ $\mu\text{H}$ ] | 0.74       | 0.67       | 0.62       | 0.57       |
| $Q_N$                   | 49.8       | 59.8       | 69.9       | 77.9       |

variation in line width ( $W$ ) and line gap ( $G$ ), the corresponding self-inductance ( $L_a$ ) and quality factor ( $Q_N$ ) of the NFC antenna are shown in Table I. With the increase in  $W$  and  $G$ , the self-inductance will decrease, whereas the quality factor will increase. According to [26], the self-inductance is required to be higher than  $0.3 \mu\text{H}$  (usually higher than  $0.5 \mu\text{H}$  by experience) for PN548 demo board and the quality factor is recommended to be higher to reduce losses. Therefore, the line width and the line gap are finally set as  $0.8$  and  $0.4$  mm for high-quality factor and acceptable self-inductance.

### B. Eddy Current Distribution

To investigate the eddy current distribution on the inner surface of the metal cover and explain the necessity for embedding the horizontal slot and rectangular slot, five cases are studied, as shown in Fig. 3. Here, the current flowing on the NFC antenna is indicated by the blue arrow line. The eddy current induced within the inner surface area of the metal cover that locates directly above the NFC antenna coil is represented by the purple arrow line, and the eddy current exhibited on the remaining surface area of the metal cover is depicted by the red arrow line.

In Case A, no clearance zone is embedded, and the NFC antenna is located at the center of the metal cover. The current on the NFC antenna coil flows clockwise, whereas all the induced eddy current (purple and red color) flows counterclockwise, which is in the reverse direction with the current flowing on the NFC antenna coil. Due to the strong reverse eddy current, the corresponding self-inductance  $L_a$  and quality factor  $Q_N$  are very low. In Case B, a horizontal slot is introduced at the center of the metal cover. Compared with Case A, the direction of the eddy current (red color) is altered to be the same with the current on the NFC antenna, resulting in a bigger self-inductance and quality factor. However, the

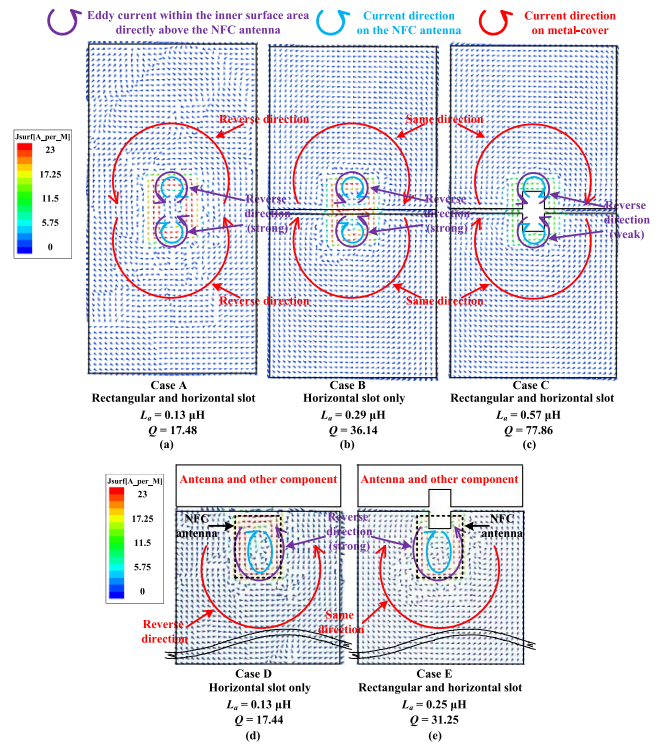


Fig. 3. Eddy current distribution of the metal cover. (a) Without clearance zone. (b) With main horizontal slot. (c) With main horizontal slot and rectangular slot. (d) With movement of the NFC antenna coil and main horizontal slot. (e) With movement of the NFC antenna coil, main horizontal slot, and rectangular slot.

eddy current (purple color) induced directly above the NFC antenna is still relatively strong. To further mitigate the eddy current (purple color), a rectangular slot is integrated on the metal cover, as shown in Case C. In this case, the self-inductance and the quality factor are as big as  $0.57$  and  $77.9$ , respectively.

In real industrial applications, the cross slot (horizontal slot and camera hole) is usually located at the top of the metal cover. In this case, the position of the NFC antenna coil may vary to make space for other antennas and components. As the NFC antenna coil moves down below the horizontal slot, Case B is transformed to Case D and Case C is transformed to Case E. Different from Case D, the eddy current (red color) of Case E is in the same direction as the current flowing on the NFC antenna coil, leading to a higher self-inductance and quality factor.

In conclusion, Case C is finally selected considering the eddy current distribution, the corresponding passive parameters ( $L_a$  and  $Q_N$ ), and the location variation in the NFC antenna coil.

## IV. CIRCUIT ANALYSIS FOR CPT

### A. Reason for Applying SN Compensation Topology

The schematic circuit model of the proposed CPT system with a general compensation circuit is shown in Fig. 4. A power amplifier is used to generate an ac source. Compensation circuits including inductance and capacitance are applied at the transmitting side and the receiving side to implement

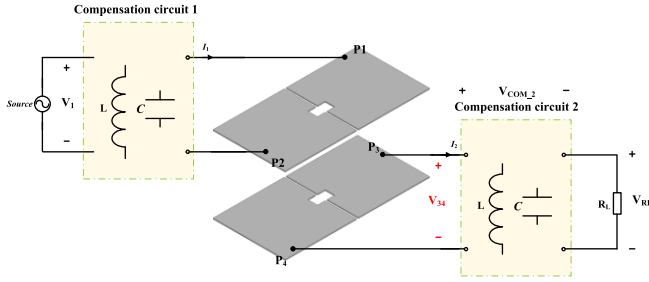


Fig. 4. Schematic circuit model of the proposed CPT system with general compensation circuit.

CPT at a desired frequency. Conventionally, the receiving metal plates are integrated inside the smartphone, making the metal-cover barrier embed between the transmitting plates and the receiving plates. To achieve CPT for metal-cover smartphone, the metal cover itself is used as the receiving plates  $P_3$  and  $P_4$  of the CPT system, which transforms the metal cover from the metal barrier to the receiving plates. Because the metal cover is used as the metal plates for CPT and people may touch it during the wireless charging process, safety issue regarding metal cover needs to be taken into consideration. According to [27] and [28], the voltage  $V_{34}$  between plates  $P_3$  and  $P_4$  shall be lower than  $V_{\text{safe}}$  (8.35 V). Here, voltage  $V_{34}$  can be expressed as

$$V_{34} = V_{RL} + V_{\text{Com}_2} \quad (1)$$

where  $V_{\text{com}_2}$  is referred to the voltage drop on the compensation circuit of the receiving side. Assuming the output power on the load resistance  $R_L$  is  $P$ , the relationship between  $V_{34}$  and  $P$  can be depicted as

$$\sqrt{PR_L} + V_{\text{Com}_2} = V_{34} < V_{\text{safe}}. \quad (2)$$

With a fixed load resistance  $R_L$ , the output power can be enhanced with a lower voltage drop  $V_{\text{Com}_2}$  on the compensation circuit. Therefore, the voltage drop on the compensation circuit needs to be decreased to gain more output power and the best way is to remove the compensation circuit on the receiver side. Besides, the self-capacitance of the receiver is very small because of the horizontal placement of plates  $P_3$  and  $P_4$ . Without external parallel capacitance, the value of the compensation inductance inside the smartphone will be very large, leading to increased loss and occupying a lot of space. Due to the space limitation inside the smartphone, the removal of the compensation components at the receiving side makes the capacitive charging system compact and significantly saves space for the smartphone.

### B. Circuit Analyses for the SN Compensation Topology

To remove the internal compensation components inside the smartphone, an SN compensation topology for CPT is proposed and the equivalent circuit is shown in Fig. 5. Only a series inductance  $L$  is integrated at the transmitting side and no compensation components are applied at the receiving side. Based on [11], the simplified  $\pi$  model including coupling capacitance  $C_M$ , self-capacitance  $C_1$ , and  $C_2$  can be used to represent the capacitive coupler. The relationship between the

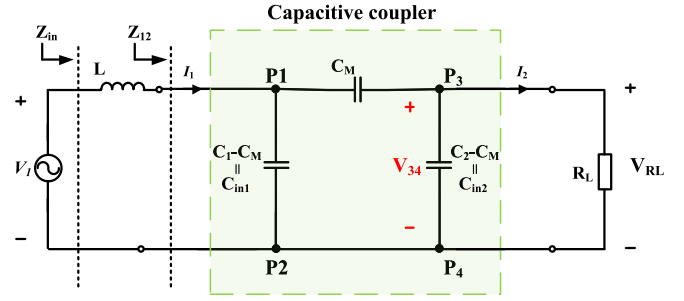


Fig. 5. Circuit diagram of the proposed CPT system with the SN compensation topology.

six capacitances ( $C_{12}$ ,  $C_{13}$ ,  $C_{14}$ ,  $C_{23}$ ,  $C_{24}$ , and  $C_{34}$ ) generated among the four metal plates and the equivalent capacitance ( $C_M$ ,  $C_1$ , and  $C_2$ ) can be described as follows:

$$\begin{cases} C_1 = C_{12} + \frac{(C_{13} + C_{14}) \cdot (C_{23} + C_{24})}{C_{13} + C_{14} + C_{23} + C_{24}} \\ C_2 = C_{34} + \frac{(C_{13} + C_{23}) \cdot (C_{14} + C_{24})}{C_{13} + C_{14} + C_{23} + C_{24}} \\ C_M = \frac{C_{24}C_{13} - C_{14}C_{23}}{C_{13} + C_{14} + C_{23} + C_{24}} \end{cases} \quad (3)$$

By selecting node  $P_2$  and node  $P_4$  as the reference, the voltage  $V_{P1}$  on node  $P_1$  and voltage  $V_{P3}$  on node  $P_3$  represent the voltage between plates  $P_1$  and  $P_2$  and the voltage between  $P_3$  and  $P_4$ , respectively. Kirchhoff's current law (KCL) can be applied on nodes 1 and 3 and the corresponding equations are expressed as

$$\begin{cases} (1 - \omega^2 LC_1 - \omega^2 LC_M)V_{P1} + \omega^2 LC_M V_{P3} = V_1 \\ -j\omega C_M V_{P1} + (j\omega C_M + j\omega C_2 + Y_{RL})V_{P3} = 0 \end{cases} \quad (4)$$

Here,  $Y_{RL}$  is the admittance of load  $R_L$ . The voltages  $V_{P1}$  and  $V_{P3}$  can be obtained as

$$\begin{cases} V_{P1} = V_1 \frac{-Y_{RL} - j\omega C_2}{(\omega^2 LC_1 - 1)Y_{RL} - j\omega C_2 + j\omega^3 LS} \\ V_{P3} = V_1 \frac{-j\omega C_M}{(\omega^2 LC_1 - 1)Y_{RL} - j\omega C_2 + j\omega^3 LS} \end{cases} \quad (5)$$

where  $S$  represents  $C_1 C_2 - C_M^2$ .

With (5), the input impedance  $Z_{in}$  of the circuit is calculated as

$$\begin{aligned} Z_{in} &= j \frac{(\omega^2 LC_1 Y_{RL} - Y_{RL} - j\omega C_2 + j\omega^3 LS)[\omega C_1 Y_{RL} - j\omega^2 S]}{(\omega C_1 Y_{RL})^2 + \omega^4 S^2} \end{aligned} \quad (6)$$

The phase angle  $\theta$  of the input impedance  $Z_{in}$  can be expressed as

$$\theta = \arctan \frac{(\omega^2 LC_1 Y_{RL} - Y_{RL})C_1 Y_{RL} - [\omega C_2 - \omega^3 LS]\omega S}{(\omega^2 LC_1 Y_{RL} - Y_{RL})\omega S + (\omega C_2 - \omega^3 LS)C_1 Y_{RL}} \quad (7)$$

The circuit efficiency of the capacitive coupler can be calculated as (8), shown at the bottom of the next page, where  $Q$  is the quality factor of the compensation inductance  $L$ . Here, the efficiency of the capacitive coupler refers to the circuit efficiency of Fig. 5, including the compensation inductor  $L$

and the capacitive coupler. For brevity, the circuit efficiency of Fig. 5 is replaced by the circuit efficiency in the rest of this article.

With  $V_{P3}$  of (5), the output power can be calculated as

$$P_{\text{out}} = V_1^2 \frac{\omega^2 C_M^2 Y_{\text{RL}}}{(\omega^2 L C_1 - 1)^2 Y_{\text{RL}}^2 + (\omega^3 L S - \omega C_2)^2}. \quad (9)$$

1) *Constant Voltage Mode*: Because  $V_{P3}$  is the voltage across the load resistance, constant voltage (CV) charging will be achieved with

$$L_{\text{CV}} = \frac{1}{\omega^2 C_1}. \quad (10)$$

The input current  $I_{1_{\text{CV}}}$  for the CV mode can be calculated as

$$I_{1_{\text{CV}}} = \frac{V_1 - V_{P1}}{j\omega L} = V_1 \frac{j\omega S + Y_{\text{RL}} C_1}{\frac{C_M}{C_1}}. \quad (11)$$

Due to “ $j\omega S$ ,” the input current  $I_{1_{\text{V}}}$  is always ahead of the input voltage  $V_1$ , indicating that zero voltage switching (ZVS) cannot be realized. Therefore, CV charging is not suitable for the proposed SN topology for CPT.

2) *Constant Current Mode*: From (5), the condition for constant current (CC) charging can be derived as

$$L_{\text{CC}} = \frac{C_2}{\omega^2 S}. \quad (12)$$

The input current  $I_{1_{\text{CC}}}$  for the CC mode can be calculated as

$$\begin{aligned} I_{1_{\text{CC}}} &= \frac{V_1 - V_{P1}}{j\omega L} \\ &= V_1 \frac{1}{Y_{\text{RL}} L_{\text{CC}}} \frac{C_2 - j\omega L_{\text{CC}} Y_L C_1}{L_{\text{CC}} \omega^2 C_1 - 1}. \end{aligned} \quad (13)$$

From (13), the input impedance  $Z_{\text{in}_{\text{CC}}}$  of the circuit can be calculated as

$$Z_{\text{in}_{\text{CC}}} = \frac{V_1}{I_{1_{\text{CC}}}} = Y_{\text{RL}} L_{\text{CC}} [L\omega^2 C_1 - 1] \frac{C_2 + j\omega L_{\text{CC}} Y_{\text{RL}} C_1}{C_2^2 + \omega^2 L_{\text{CC}}^2 Y_{\text{RL}}^2 C_1^2}. \quad (14)$$

The phase angle  $\theta_{\text{CC}}$  of the input impedance can be expressed as

$$\theta_{\text{CC}} = \arctan \frac{Y_{\text{RL}} C_1}{\omega S}. \quad (15)$$

Due to the symmetric capacitive coupler structure,  $C_1 = C_2 > C_M$  is obtained for the proposed coupler, leading to  $\theta_{\text{CC}} > 0$ . Therefore, the input current  $I_{1_{\text{CC}}}$  will always lag behind the input voltage  $V_1$ , indicating that ZVS can be achieved with CC charging if an inverter is applied for the input ac power. From (5), (12), and (13), the circuit efficiency of the capacitive coupler can be calculated as

$$\eta_{\text{CC}} = \frac{\frac{V_{P3}^2}{R_L}}{\frac{V_{P3}^2}{R_L} + I_{1_{\text{CC}}}^2 R_1} = \frac{\omega(C_M)^2 Y_{\text{RL}}}{\omega(C_M)^2 Y_{\text{RL}} + \left[ \frac{C_2}{S} Y_{\text{RL}}^2 C_1^2 + \omega^2 S C_2 \right] \frac{1}{Q}}. \quad (16)$$

To achieve the maximum circuit efficiency, three methods can be applied, that is, 1) tuning the load resistance  $R_L$ ; 2) adding external parallel capacitance  $C_{2_{\text{ext}}}$  between plates  $P_3$  and  $P_4$ ; and 3) adding external capacitance  $C_{1_{\text{ext}}}$  between plates  $P_1$  and  $P_2$ .

From (16), the optimum resistance  $R_{\text{LO}_{\text{CC}}}$  for the maximum efficiency can be calculated as

$$R_{\text{LO}_{\text{CC}}} = \frac{C_1}{\omega S}. \quad (17)$$

In the proposed capacitive coupler,  $C_1$ ,  $C_2$ , and  $C_M$  are all several nanofarads and the frequency of the system is several megahertz. At the desired 6.78-MHz working frequency, the calculated  $R_{\text{LO}_{\text{CC}}}$  will be over 50  $\Omega$ . However, with safety consideration, the load resistance should be

$$R_L \leq \frac{V_{\text{safe}}^2}{P}. \quad (18)$$

With a 5-W output power, the largest load resistance  $R_L$  is calculated to be 14  $\Omega$ , which is much smaller than  $R_{\text{LO}_{\text{CC}}}$ . Therefore, the load resistance cannot be tuned to achieve the maximum efficiency for the proposed capacitive coupler. Within a safety range, the circuit efficiency will increase with the increase in load resistance.

If an additional capacitance  $C_{2_{\text{ext}}}$  is added in parallel with plates  $P_3$  and  $P_4$ , (16) should be revised as

$$\eta_{\text{CC}} = \frac{\omega(C_M)^2 Y_{\text{RL}}}{\omega(C_M)^2 Y_{\text{RL}} + \left[ \frac{C_2 + C_{2_{\text{ext}}}}{C_1(C_2 + C_{2_{\text{ext}}}) - C_M^2} Y_{\text{RL}}^2 C_1^2 + \omega^2 (C_1 C_2 + C_1 C_{2_{\text{ext}}} - C_M^2) \times (C_2 + C_{2_{\text{ext}}}) \right] \frac{1}{Q}}. \quad (19)$$

By solving  $\partial \eta / \partial C_{2_{\text{ext}}} = 0$  and defining  $d$ ,  $u$ , and  $v$  as

$$\begin{cases} d = -Y_{\text{RL}}^2 C_1^2 \frac{C_M^2}{\omega^2} \\ u = \frac{54d - C_M^6}{216} \\ v = \frac{\sqrt{3(27d^2 + C_M^6 d)}}{36} \\ m = \sqrt[3]{v - u}, n = \frac{C_M^4}{18m} \\ x = m + n - \frac{C_M^2}{6}. \end{cases} \quad (20)$$

The optimum  $C_{2_{\text{ext}}}$  for the maximum efficiency can be calculated as

$$C_{2_{\text{ext}}} = \frac{x + C_M^2}{C_1} - C_2. \quad (21)$$

Because  $C_{2_{\text{ext}}}$  is in parallel with  $P_3$  and  $P_4$ , additional capacitance components need to be integrated into the smartphone, which is not preferable and feasible for a compact smartphone.

$$\eta = \frac{(\omega^2 L C_1 Y_{\text{RL}} - Y_{\text{RL}}) S + (C_2 - \omega^2 L S) C_1 Y_{\text{RL}}}{(\omega^2 L C_1 Y_{\text{RL}} - Y_{\text{RL}}) S + (C_2 - \omega^2 L S) C_1 Y_{\text{RL}} + (\omega(C_1 Y_{\text{RL}})^2 + \omega^3 S^2) \frac{L}{Q}}, \quad (8)$$

With an additional capacitance  $C_{1\_ext}$  in parallel with plates  $P_1$  and  $P_2$ , the efficiency can be calculated as

$$\eta_{CC} = \frac{\omega(C_M)^2 Y_{RL}}{\omega(C_M)^2 Y_{RL} + \left[ \frac{C_2}{(C_1 + C_{1\_ext})C_2 - C_M^2} Y_{RL}^2 (C_1 + C_{1\_ext})^2 + \omega^2(C_1 C_2 + C_{1\_ext} C_2 - C_M^2) C_2 \right] \frac{1}{Q}}. \quad (22)$$

Let  $\partial\eta/\partial C_{1\_ext} = 0$  and  $f = Y_{RL}^2 + \omega^2 C_2^2$ , the optimum  $C_{1\_ext}$  for the maximum efficiency is expressed as

$$C_{1\_ext} = \frac{C_M^2 f + \sqrt{C_M^4 f^2 - \omega^2 C_2^2 C_M^4 f}}{C_2 f} - C_1. \quad (23)$$

Here, the external capacitance  $C_{1\_ext}$  is embedded in the transmitter where space is not strictly limited. Therefore, adding external capacitance  $C_{1\_ext}$  is a possible and applicable way to achieve the maximum efficiency (CC mode) for the proposed capacitive system in view of compact space inside the smartphone.

3) *Zero Phase Angle Mode*: If the inductance  $L$  is used to compensate the reactance of the impedance  $Z_{12}$ , zero phase angle (ZPA) can be achieved. Here, the inductive reactance of  $L$  can be tuned slightly bigger than the imaginary part of  $Z_{12}$  to achieve ZVS if an inverter is used. To analyze the characteristic of the circuit for ZPA, let  $\text{imag}(Z_{in}) = 0$  and the corresponding compensated inductance  $L_{ZPA}$  is derived as

$$L_{ZPA} = \frac{\omega^2 C_2 S + Y_{RL}^2 C_1}{\omega^2 Y_{RL}^2 C_1^2 + \omega^4 S^2}. \quad (24)$$

The circuit efficiency  $\eta_{ZPA}$  can be calculated as

$$\eta_{ZPA} = \frac{\omega C_M^2}{\omega C_M^2 + \frac{\omega^2 C_2 S + Y_{RL}^2 C_1}{Q}}. \quad (25)$$

Based on (25), the optimum load resistance  $R_L$  for the maximum efficiency can be derived as

$$R_{LO\_ZPA} = \sqrt{\frac{C_1}{\omega^2 C_2 S}}. \quad (26)$$

Because  $C_1$ ,  $C_2$ , and  $C_M$  are all in a range of several hundred picofarads, and the desired working frequency is several megahertz, the optimum load resistance  $R_{LO\_ZPA}$  will be several hundred ohms, which has exceeded the safety voltage requirement by (18). Therefore, the load resistance  $R_L$  needs to be smaller than  $R_{LO\_ZPA}$  and the efficiency will increase with the increase in load resistance within the safety range.

### C. Comparison Between CC Mode With External Capacitance $C_{1\_ext}$ and ZPA Mode

As indicated in Section IV-B, adding an additional parallel capacitor  $C_{1\_ext}$  is the most applicable and reasonable way to achieve the maximum efficiency for CC mode charging. Thus, the CC mode without an external capacitance, the CC mode with an external capacitance  $C_{1\_ext}$ , and the ZPA mode

TABLE II  
SIMULATED PARAMETERS OF THE CPT-NFC-COMBINED COUPLER WITH DIFFERENT DIELECTRIC MATERIALS

| Parameters   | Dielectric material |        |        |        |        |
|--------------|---------------------|--------|--------|--------|--------|
|              | Ro3010              | TMM 10 | Ro3006 | Glass  | FR4    |
| $\epsilon_r$ | 10.2                | 9.2    | 6.15   | 5.5    | 4.4    |
| $C_M$ [pF]   | 394.8               | 356.9  | 237.6  | 212.6  | 174.3  |
| $C_1$ [pF]   | 396.8               | 359.1  | 238.8  | 213.7  | 176.6  |
| $\eta$       | 94.48%              | 93.92% | 91.15% | 90.21% | 88.23% |

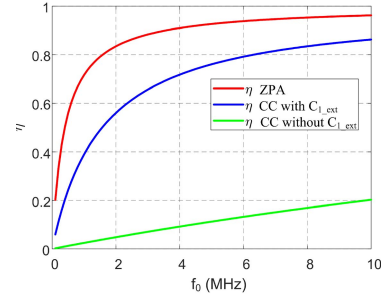


Fig. 6. Circuit efficiency  $\eta$  of the proposed capacitive coupler operating at the ZPA mode and CC mode.

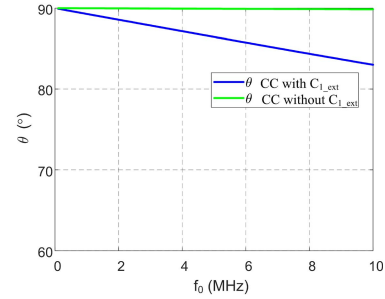


Fig. 7. Phase angle  $\theta_{CC}$  of the input impedance for the CC mode with or without external capacitor  $C_{1\_ext}$ .

are studied in this section. For fair comparison, a fixed load resistance ( $10 \Omega$ ) within the safety range is used for calculation. It is noteworthy that the quality factor is predicted by experience at the first stage and the measured quality factor of 102.3 is used here for calculation. With passive parameters of the capacitive coupler listed in Table II, the corresponding circuit parameters are calculated and the results are shown in Figs. 6–12. The circuit efficiency  $\eta_{CC}$  for the CC mode without an external capacitance, the CC mode with an external capacitance  $C_{1\_ext}$ , and  $\eta_{ZPA}$  for the ZPA mode are calculated by (16), (22), and (25), respectively. As shown in Fig. 6, the efficiency of the ZPA mode is always higher than the CC mode with or without an external capacitor at different working frequencies.

Based on (15) and (23), the phase angle  $\theta_{CC}$  of the input impedance for the CC mode is depicted in Fig. 7. At different working frequencies,  $\theta_{CC}$  is all above  $80^\circ$ , leading to a relatively high reactive power. As a result, with the same output power, the input power and the voltage rating of the components for the CC mode will be higher than the ZPA mode.

As for compensation inductance,  $L_{CC}$  without an external capacitance will be much larger than  $L_{CC}$  with an external capacitance so that only  $L_{CC}$  with external capacitance  $C_{1\_ext}$

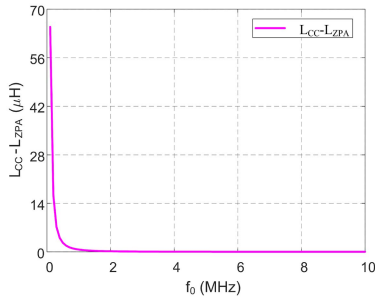


Fig. 8. Difference of compensation inductance between  $L_{ZPA}$  of the ZPA mode and  $L_{CC}$  of the CC mode.

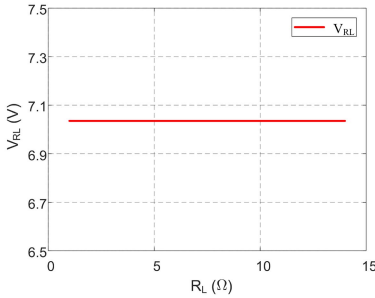


Fig. 9. Variation in load voltage regarding load resistance in the ZPA mode.

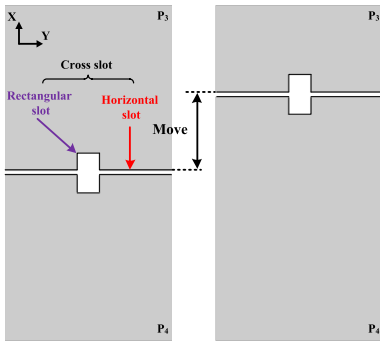


Fig. 10. Movement of the cross slot for investigation of capacitance variation.

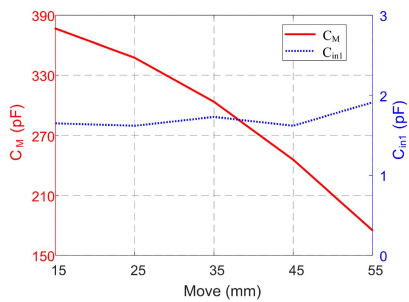


Fig. 11. Variation in the coupling capacitance  $C_M$  and capacitance  $C_{in1}$  regarding movement of the cross slot.

is depicted for comparison. According to (12), (23), and (24), the compensation inductance  $L_{CC}$  for the CC mode with an external capacitance and  $L_{ZPA}$  for the ZPA mode are calculated and the corresponding differences between  $L_{CC}$  and  $L_{ZPA}$  are shown in Fig. 8. It can be seen that the compensation inductance  $L_{CC}$  is always higher than  $L_{ZPA}$ , especially at relatively low-frequency range. Thus, the volume of  $L_{CC}$  will be larger compared with  $L_{ZPA}$ , which does not meet the compact requirement by smartphone applications.

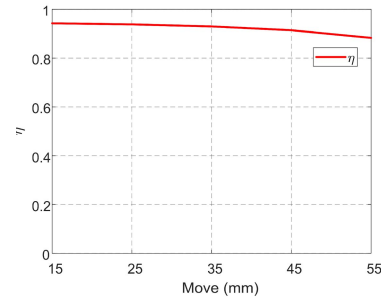


Fig. 12. Variation in the circuit efficiency  $\eta$  regarding movement of the cross slot.

In addition, because no external parallel capacitance is used for the ZPA mode,  $C_{in1}$  and  $C_{in2}$  are very small. Compared with  $Y_{RL}^2 C_1$  and  $\omega^2 Y_{RL}^2 C_1^2$ ,  $\omega^2 C_2 S$  and  $\omega^4 S^2$  are much smaller in this case, and (24) can thus be approximated as (27), leading to CV charging for the ZPA mode

$$L_{ZPA} = \frac{\omega^2 C_2 S + Y_{RL}^2 C_1}{\omega^2 Y_{RL}^2 C_1^2 + \omega^4 S^2} \approx \frac{Y_{RL}^2 C_1}{\omega^2 Y_{RL}^2 C_1^2} = L_{CV}. \quad (27)$$

To verify this, a constant input voltage of 7 V is set for calculation. As the load resistance varies between 1 and 14  $\Omega$ , the output voltage derived by (5) and (24) is nearly constant, as shown in Fig. 9. Above all, CV charging is actually achieved with the ZPA mode for the proposed NFC-CPT-combined coupler.

Considering efficiency, phase angle, compensation inductance, and output property, the ZPA mode is better than the CC mode for the proposed capacitive coupler with the SN topology. Because the proposed capacitive coupler is horizontally arranged with no parallel external capacitance, the compensation inductance  $L_{ZPA}$  will be too large to be embedded in the transmitter at low operating frequency. According to industrial, scientific, and medical (ISM) radio bands, a relatively high working frequency of 6.78 MHz is selected as the working frequency. In conclusion, the SN topology with the ZPA mode is the most suitable compensation topology and it is applied at 6.78-MHz working frequency to the proposed capacitive coupler.

## V. CAPACITIVE COUPLER DESIGN

In this section, ANSYS Maxwell is used to analyze the proposed capacitive coupler. Because the metal cover of the smartphone is used as the receiving plates for the capacitive charging system, the planar size of one metal plate is set as 74 mm  $\times$  75 mm based on the size of an actual smartphone. To mitigate the eddy current loss for NFC antenna and achieve NFC through the metal cover, a width horizontal slot and a rectangular slot are integrated on the metal plates, which determine the shape of the capacitive metal plates. The main horizontal slot contributes to the clearance for LTE/WWAN antennas whose width is usually within 3 mm. A relatively small slot width of 2 mm is selected for the proposed coupler. In a commercial metal-cover smartphone, the rectangular slot normally represents the camera hole and flash hole. To achieve appropriate passive parameters, the size of the rectangular slot

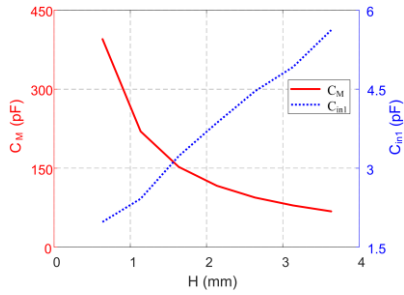


Fig. 13. Variation in the coupling capacitance  $C_M$  and capacitance  $C_{in1}$  regarding thickness  $H$  of the dielectric layer Ro3010.

is set as  $18 \text{ mm} \times 10 \text{ mm}$  in consideration of the actual size of camera and flashlight.

In a commercial smartphone, the location of the cross slot varies for different smartphones. Because the transmitting plates ( $P1$  and  $P2$ ) are identical to the receiving plates ( $P3$  and  $P4$ ), the movement of the cross slot for the transmitting plates will be the same as the receiving plates. As the cross slot moves along the  $X$ -axis of Fig. 10, the variation in coupling capacitance  $C_M$  and capacitance  $C_{in1}$  derived by (3) and (28) is shown in Fig. 11. Here,  $C_{in1}$  is defined as

$$C_{in1} = C_1 - C_M. \quad (28)$$

Based on (25), the circuit efficiency (ZPA mode) is calculated and the corresponding results are shown in Fig. 12. As the cross slot of both the transmitting and the receiving plates move away from the center of the metal cover, the coupling capacitance  $C_M$  will decrease and  $C_{in1}$  will nearly remain the same. Here, the calculated efficiency changes from 88.3% to 94.2% with the position variation in the cross slot, indicating that the proposed CPT coupler can be applied to smartphones with different metal-cover layout. For research purpose, the cross slot is located at the center of the transmitting and the receiving metal plates for best efficiency.

As for the dielectric layer of the transmitter, the material and thickness  $H$  are investigated. Integrated with different materials, the coupling capacitance  $C_M$ , self-capacitance  $C_1$ , and efficiency  $\eta$  (ZPA mode) are simulated and the corresponding results are listed in Table II. Here, self-capacitance  $C_2$  equals  $C_1$  due to the symmetrical structure of the capacitive coupler. It can be seen that the material with a higher dielectric constant can achieve a higher coupling capacitance, leading to high efficiency. With the increase in thickness  $H$ , the coupling capacitance  $C_M$  will decrease and the capacitance  $C_{in1}$  will increase, leading to low efficiency, as shown in Fig. 13. Considering the performance, cost, and availability, Ro3010 of 0.635 mm thickness is used to fabricate the transmitter.

With the defined  $X$ - and  $Y$ -axes in Fig. 1, the misalignment ability regarding the  $X$ - and  $Y$ -axes is studied. Because the transmitter is composed of the transmitting plates ( $P_1$ ,  $P_2$ ) and the Ro3010 dielectric layer, the receiving plates ( $P_3$ ,  $P_4$ ) are moved along the  $X$ - and  $Y$ -axes during the study. When there is a displacement misalignment, the capacitances  $C_M$  and  $C_{in1}$  are simulated as Fig. 14(a) and (b), respectively. With the

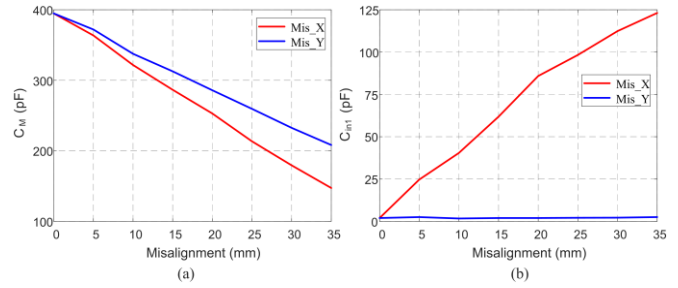


Fig. 14. (a) Coupling capacitance  $C_M$  and (b) capacitance  $C_{in1}$  of the NFC-CPT-combined coupler regarding  $X$ - and  $Y$ -axes misalignment.

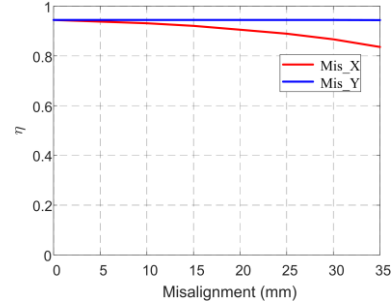


Fig. 15. Circuit efficiency  $\eta$  of the NFC-CPT-combined coupler regarding  $X$ - and  $Y$ -axes misalignment.

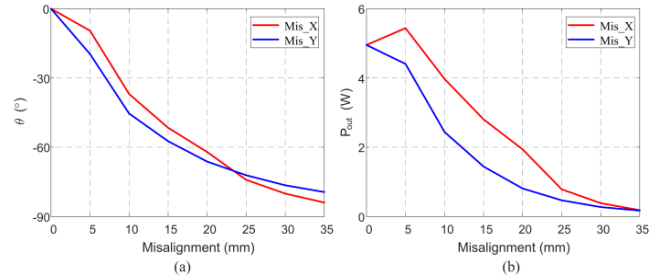


Fig. 16. (a) Phase angle  $\theta$  and (b) output power  $P_{out}$  of the NFC-CPT-combined coupler regarding  $X$ - and  $Y$ -axes misalignment.

increase in  $X$  misalignment, the coupling capacitance  $C_M$  will decrease, whereas the capacitance  $C_{in1}$  will increase. With the increase in  $Y$  misalignment, the coupling capacitance  $C_M$  will decrease, whereas the capacitance  $C_{in1}$  is nearly unchanged. Fig. 14(a) shows that  $C_M$  can maintain higher than 50% of the nominal value when  $Y$  misalignment increases to 35 mm. Compared with  $Y$  misalignment, capacitances vary bigger due to  $X$  misalignment, especially the capacitance  $C_{in1}$ .

With  $V_1$  of 7 V,  $L$  of  $1.39 \mu\text{H}$ ,  $R_L$  of  $10 \Omega$ , and capacitances at different misalignment, the circuit efficiency  $\eta$ , phase angle  $\theta$ , and output power  $P_{out}$  are calculated by (8)–(9), respectively. The corresponding results are shown in Figs. 15 and 16(a) and (b). The corresponding circuit efficiency will decrease with  $X$  misalignment and nearly remain unchanged with  $Y$  misalignment. The amplitude of the phase angle between the input voltage and current will increase significantly with  $X$  and  $Y$  misalignment, leading to reduced input and output power. Here, the output power is increased at  $Mis\_X = 5 \text{ mm}$  because a voltage source  $V_1$  is applied here for analysis, leading to an increased input power due to increased  $C_{in1}$ .

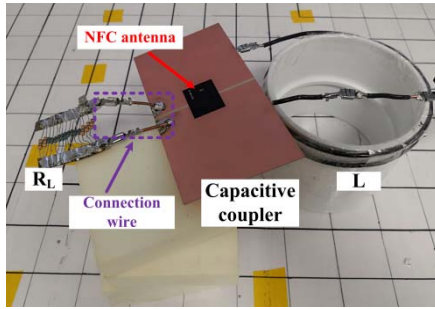


Fig. 17. Fabricated prototype of the proposed CPT-NFC-combined coupler.

## VI. CORRELATION AND INFLUENCE BETWEEN NFC AND CPT

Because the NFC antenna and capacitive coupler are integrated in a compact smartphone, the correlation and influence between them are discussed in the following paragraph, respectively.

As stated in Section III, to achieve NFC through a metal cover, a horizontal slot and a rectangular slot need to be embedded on the metal cover. This cross slot divides the metal cover into two separate metal plates, which helps make the metal cover to be the receiving coupler  $P_3$  and  $P_4$  for CPT. That is because two separate metal plates are required for the receiver of a CPT system. On the other hand, the eddy current loss of the NFC antenna is mitigated by the irregular shape of the receiving metal plates so that the NFC antenna also benefits from the capacitive coupler.

Because the two metal plates are simulated with the NFC antenna in Section III, the impact of the capacitive coupler on the NFC antenna has already been taken into consideration. To investigate the influence of the NFC antenna on the capacitive coupler, the coupling capacitance  $C_M$  and self-capacitance  $C_1$  with integrated NFC antenna are simulated as 392.9 and 397.8 pF, respectively. Compared with the results without NFC antenna in Table II, it can be concluded that the NFC antenna has very little impact on the capacitive coupler. That is because the planar size of the NFC antenna is only 30 mm  $\times$  22 mm, which only occupies 5.9% of the metal-cover area.

In conclusion, the NFC antenna and capacitive coupler benefit from each other. The influence on the NFC antenna from the capacitive coupler has already been taken into consideration at first design stage and the influence from NFC antenna on the capacitive coupler is negligible.

## VII. EXPERIMENT AND DISCUSSION

The prototype of the proposed NFC-CPT-combined coupler for smartphone applications was fabricated and tested, as shown in Fig. 17. The Ro3010 substrate ( $\epsilon_r = 10.2$ ) of 0.635-mm thickness was sandwiched between the transmitting plates and the receiving plates, constructing the capacitive coupler. To mitigate the eddy current loss and realize NFC, the transmitting plate and the receiving plate were both separated by cross slot composing of a main horizontal slot and a rectangular slot. For the purpose

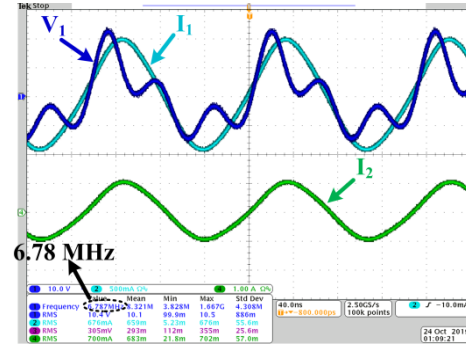


Fig. 18. Experimental waveforms of the proposed NFC-CPT-combined coupler for the ZPA mode.

TABLE III  
MEASURED PARAMETERS OF THE PROPOSED  
NFC-CPT-COMBINED COUPLER

| Parameter | Value        | Parameter | Value          |
|-----------|--------------|-----------|----------------|
| $C_M$     | 413.94 pF    | $C_1$     | 425.86 pF      |
| $L$       | 1.32 $\mu$ H | $R_L$     | 10.19 $\Omega$ |
| $Q$       | 102.3        |           |                |

of increasing the quality factor and reducing the loss at 6.78-MHz working frequency, compensation air core coil  $L$  was fabricated by Reminton 12SLDDBLATHHN50 12 AWG gauge solid wire of 2.053-mm diameter [29]. Here, the plastic tube does not change the inductance because it is not made up of ferromagnetic (like ferrite) and metallic (like copper) material. On the top of the stack, the NFC antenna coil was glued at the center of the two receiving metal plates. Here, the NFC antenna coil was fabricated by flexible printed circuit board (FPCB) with polyimide (PI,  $\epsilon_r = 3$ ) base material.

### A. Experiment on the Capacitive Coupler

For the experiment of the capacitive coupler, the 6.78-MHz ac power was provided by AG 1016 from T&C Power. Because the SN compensation topology was applied, the load resistance  $R_L$  was directly connected to the receiving plates. The corresponding measured parameters of the capacitive coupler are listed in Table III. A relatively big coupling capacitance  $C_M$  of 413.9 pF was realized between the transmitting plates and the receiving plates. To achieve ZPA, the compensation inductance  $L$  was fabricated to be 1.32  $\mu$ H.

Because the passive parameters (inductance, capacitance, and resistance) of the proposed coupler do not change with the variation in the output power level, the circuit efficiency is not correlative with the output power based on (25). Because the output power does not affect the circuit efficiency, only one power level is tested. With 5-W output power, the experimental waveforms are shown in Fig. 18. The circuit efficiency of the proposed CPT-NFC-combined coupler was measured to be 93.5%. ZPA had been achieved at 6.78 MHz and the voltage across the receiving plates was validated to be 7.75 V with a 5-W output power, which met the safety voltage (8.35 V) requirement. Because the receiving metal plates were parallel

TABLE IV  
COMPARISON OF COMMON METRICS FOR  
SMALL-POWER CPT

| Reference | Output power [W] | Efficiency [%]   | Frequency [MHz] | Gap [mm] | Plate area [cm <sup>2</sup> ] |
|-----------|------------------|------------------|-----------------|----------|-------------------------------|
| [7]       | 4                | 16               | 1.237           | 0.2      | 25                            |
| [8]       | 40               | 44.3             | 0.217           | 1        | 54                            |
| [13]      | 1.6              | 54               | 0.449           | 0.5      | 100                           |
| [14]      | 15               | 52~58<br>(AC-AC) | 3.45            | 1.5      | 380.25                        |
| [32]      | 0~1.46           | ≈ 81<br>(AC-AC)  | 1               | 0.4      | 100                           |
| [33]      | 260              | 79               | 0.5             | 0.2      | 200                           |
| [34]      | 3.7              | 80               | 4.2             | 0.13     | 6                             |
| [35]      | 6.5              | 94.3             | 0.626           | 0.8      | 653                           |
| [36]      | 7.6              | 41               | 0.84            | 1        | 100                           |
| proposed  | 5.6              | 93.5<br>(AC-AC)  | 6.78            | 0.635    | 55.5                          |

connected with the load resistance, the voltage across the metal cover should be 7.16 V with a 5-W output power. Here, the measured voltage of 7.75 V is higher than the calculated value because it includes a voltage drop on the connection wire. Because the working frequency is relatively high at 6.78 MHz, the voltage drop on the connection wire will be relatively high. It is noteworthy that this connection wire is necessary for experiment but will be removed in real applications so that the voltage on the metal cover will be reduced in practical applications.

The power loss of the NFC-CPT-combined coupler mainly comes from the compensation inductance and the capacitive coupler. Based on the input current of Fig. 18 and the parameters from Table III, the power loss of the inductance can be calculated as 0.251 W, which dissipates 72.5% of the total power loss. Here, the rest of the power loss comes from the capacitive coupler due to the Ro3010 dielectric layer with 0.0022 dissipation factor.

Because the proposed capacitive coupler is designed for small-power consumer electronics, the comparison on common metrics for small-power applications is necessary to be listed in Table IV. Here, the gap between the transmitter and the receiver indicates the transmission range of the capacitive coupler. The circuit efficiency of a capacitive coupler is determined by the quality factor of the compensation coil, the coupler itself (dielectric material, gap, and plate material), and the value of the load resistance. With the increase in dielectric layer permittivity, decrease in gap, and increase in plate area, the coupling capacitance  $C_M$  will increase, leading to enhanced circuit efficiency. For small-power capacitive coupler, the plate area and output power are set based on designated applications. Because the receiving plates are placed directly on the dielectric layer for small-power applications, the gap and dielectric material can be varied to achieve the desired efficiency. Objectively speaking, all the references and the proposed capacitive coupler follow the same design principle. Although the proposed capacitive coupler achieves relatively high circuit efficiency with a relatively small plate area, it cannot be viewed as an advantage over

TABLE V  
DETECTION RANGE OF FOUR TYPE OF CARDS

| Card Type            | Type 1 | Type 2 | Type 3 | Type 4 |
|----------------------|--------|--------|--------|--------|
| Detection Range [mm] | 61     | 55     | 37     | 29     |

\*Type 1 and Type 2 Tags are based on ISO/IEC 14443A. Type 3 Tag is based on JIS, also known as FeliCa. Type 4 Tag is fully compatible with the ISO/IEC 14443 A/B standard series [30]

TABLE VI  
COMPARISONS OF NFC ANTENNA DIMENSION, CLEARANCE  
ZONE, AND DETECTION RANGE

| Scheme             | Antenna Dimension [mm <sup>3</sup> ] | Clearance Zone [mm <sup>2</sup> ] | Detection Range [mm] |
|--------------------|--------------------------------------|-----------------------------------|----------------------|
| Lee et al. [16]    | 39 × 51 × 0.017                      | Non-metallic                      | 56                   |
| Zhao et al. [18]   | 6 × 3 × 1                            | Non-metallic                      | 34                   |
| Zhu et al. [22]    | 38.6 × 46 × 0.035                    | 74 × 2                            | 50                   |
| Zhu et al. [23]    | 15 × 25 × 0.035                      | 8 × 16                            | 21                   |
| Zhu et al. [25]    | 60 × 11 × 0.035                      | 75 × 2                            | 53                   |
| Chung et. al. [31] | 41.5 × 7.5 × 0.45                    | >41.5 × 7.5                       | 65                   |
| Proposed           | 30 × 22 × 0.035                      | 65 × 2<br>& 18 × 10               | 61                   |

other references because of the applied Ro3010 substrate ( $\epsilon_r = 10.2$ ,  $\tan\delta = 0.0022$ ) and the medium gap distance.

### B. Experiment on the NFC Antenna

For the experiment of the NFC antenna, the detection range of four standard NFC forum cards [30] was tested for read/write (R/W) mode. The self-inductance ( $L_a$ ) at 1-MHz, dc resistance ( $R_s$ ) at 1 MHz, and quality factor ( $Q_N$ ) at 13.56 MHz of the proposed NFC antenna were measured to be 0.65  $\mu$ H, 0.73  $\Omega$ , and 18.2, respectively.

Together with the metal cover (receiving plates), the NFC antenna was connected to the PN548 demo board through a coaxial line [26]. Because the balanced (differential) analog circuit was applied on the demo board, two series capacitors of 82 pF//8.2 pF and two parallel capacitors of 180 pF//180 pF were adopted. Here, the symbol // is denoted as parallel. To conduct R/W mode test, the PN548 demo board was in conjunction with a computer through a USB cable. The corresponding R/W mode test results are listed in Table V. Here, the detection range of Type 1 to Type 4 varies from 29 to 61 mm, which are good and enough for daily use. For comparison purpose, the antenna dimension, clearance zone, and detection range for different schemes are listed in Table VI. Here, the ferrite and metal mainboard are not included for NFC in this article. From Table VI, it can be concluded that the proposed NFC antenna achieves a good detection range with a medium antenna dimension and relatively big clearance zone.

## VIII. CONCLUSION

In this article, an NFC-CPT-combined coupler with the SN compensation topology is proposed for metal-cover smartphones. A main horizontal slot of 2-mm width and a rectangular slot of 18 mm × 10 mm are loaded on the metal cover, dividing the metal cover into two separate metal plates. The separate metal plates are used as the receiving metal

plates, thus achieving CPT through a metal cover. By placing the NFC antenna at the center of the metal cover and optimizing the size and shape of the metal plates, the eddy current loss is mitigated and NFC through a metal cover is realized. At 6.78-MHz working frequency, a 1.32- $\mu$ H series inductance is applied at the transmitting side and no compensation components are integrated inside the smartphone. With 5-W output power, a 93.5% circuit efficiency is achieved and the voltage across the metal cover is 7.75 V, which meets the safety requirement. With regard to the NFC antenna, a detection range of 61 mm is obtained for the R/W mode. Because the NFC antenna and capacitive coupler benefit each other and they both achieve good performance, the proposed NFC-CPT-combined coupler is a good candidate for smartphone applications.

## REFERENCES

- [1] S. Li and C. C. Mi, "Wireless power transfer for electric vehicle applications," *IEEE J. Emerg. Sel. Topics Power Electron.*, vol. 3, no. 1, pp. 4–17, Mar. 2015.
- [2] G. A. Covic and J. T. Boys, "Modern trends in inductive power transfer for transportation applications," *IEEE J. Emerg. Sel. Topics Power Electron.*, vol. 1, no. 1, pp. 28–41, Mar. 2013.
- [3] J. Dai and D. C. Ludois, "A survey of wireless power transfer and a critical comparison of inductive and capacitive coupling for small gap applications," *IEEE Trans. Power Electron.*, vol. 30, no. 11, pp. 6017–6029, Nov. 2015.
- [4] S. Y. Hui, "Planar wireless charging technology for portable electronic products and qi," *Proc. IEEE*, vol. 101, no. 6, pp. 1290–1301, Jun. 2013.
- [5] D. J. Graham, J. A. Neasham, and B. S. Sharif, "Investigation of methods for data communication and power delivery through metals," *IEEE Trans. Ind. Electron.*, vol. 58, no. 10, pp. 4972–4980, Oct. 2011.
- [6] O. Imoru, A. Jassal, H. Polinder, E. Nieuwkoop, J. Tsado, and A. A. Jimoh, "An inductive power transfer through metal object," in *Proc. 1st Int. Future Energy Electron. Conf. (IFEEC)*, Nov. 2013, pp. 246–251.
- [7] B. H. Choi, D. T. Nguyen, S. J. Yoo, J. H. Kim, and C. T. Rim, "A novel source-side monitored capacitive power transfer system for contactless mobile charger using class-E converter," in *Proc. IEEE Vehicle Technol. Conf.*, May 2014, pp. 1–5.
- [8] A. P. Hu, C. Liu, and H. L. Li, "A novel contactless battery charging system for soccer playing robot," in *Proc. 15th Int. Conf. Mechatronics Mach. Vis. Pract.*, Dec. 2008, pp. 646–650.
- [9] L. J. Zou, Q. Zhu, C. W. V. Neste, and A. P. Hu, "Modelling single-wire capacitive power transfer system with strong coupling to ground," *IEEE J. Emerg. Sel. Topics Power Electron.*, early access, Sep. 2019, doi: 10.1109/JESTPE.2019.2942034.
- [10] F. Lu, H. Zhang, H. Hofmann, and C. Mi, "A double-sided LCLC-compensated capacitive power transfer system for electric vehicle charging," *IEEE Trans. Power Electron.*, vol. 30, no. 11, pp. 6011–6014, Nov. 2015.
- [11] H. Zhang, F. Lu, H. Hofmann, W. Liu, and C. C. Mi, "A four-plate compact capacitive coupler design and LCL-compensated topology for capacitive power transfer in electric vehicle charging application," *IEEE Trans. Power Electron.*, vol. 31, no. 12, pp. 8541–8551, Dec. 2016.
- [12] F. Lu, H. Zhang, H. Hofmann, and C. C. Mi, "A double-sided LC-compensation circuit for loosely coupled capacitive power transfer," *IEEE Trans. Power Electron.*, vol. 33, no. 2, pp. 1633–1643, Feb. 2018.
- [13] C. Liu, A. P. Hu, B. Wang, and N.-K.-C. Nair, "A capacitively coupled contactless matrix charging platform with soft switched transformer control," *IEEE Trans. Ind. Electron.*, vol. 60, no. 1, pp. 249–260, Jan. 2013.
- [14] J.-Q. Zhu *et al.*, "A novel capacitive coupler array with free-positioning feature for mobile tablet applications," *IEEE Trans. Power Electron.*, vol. 34, no. 7, pp. 6014–6019, Jul. 2019.
- [15] J. Fischer, "NFC in cell phones: The new paradigm for an interactive world," *IEEE Commun. Mag.*, vol. 47, no. 6, pp. 22–28, Jun. 2009.
- [16] B. Lee, B. Kim, F. J. Harackiewicz, B. Mun, and H. Lee, "NFC antenna design for low-permeability ferromagnetic material," *IEEE Antennas Wireless Propag. Lett.*, vol. 13, pp. 59–62, 2014.
- [17] M.-S. Wang, Y.-X. Guo, and W. Wu, "Planar shared antenna structure for NFC and UHF-RFID reader applications," *IEEE Trans. Antennas Propag.*, vol. 65, no. 10, pp. 5583–5588, Oct. 2017.
- [18] A. Zhao and F. Ai, "Dual-resonance NFC antenna system based on NFC chip antenna," *IEEE Antennas Wireless Propag. Lett.*, vol. 16, pp. 2856–2860, 2017.
- [19] X. Qing and Z. N. Chen, "Proximity effects of metallic environments on high frequency RFID reader antenna: Study and applications," *IEEE Trans. Antennas Propag.*, vol. 55, no. 11, pp. 3105–3111, Nov. 2007.
- [20] S. Nakano, "An antenna device and a communication terminal device," CN Patent 105390815 A, Mar. 9, 2016.
- [21] H. Chen and A. Zhao, "NFC antenna for portable device with metal back cover," in *Proc. IEEE APS/URSI Int. Symp.*, Jun. 2016, pp. 1471–1472.
- [22] J.-Q. Zhu, Y.-L. Ban, C.-Y.-D. Sim, and G. Wu, "NFC antenna with nonuniform meandering line and partial coverage ferrite sheet for metal cover smartphone applications," *IEEE Trans. Antennas Propag.*, vol. 65, no. 6, pp. 2827–2835, Jun. 2017.
- [23] J.-Q. Zhu, Y.-L. Ban, R.-M. Xu, C.-Y.-D. Sim, J. Guo, and Z.-F. Yu, "Miniaturized dual-loop NFC antenna with a very small slot clearance for metal-cover smartphone applications," *IEEE Trans. Antennas Propag.*, vol. 66, no. 3, pp. 1553–1558, Mar. 2018.
- [24] A. Zhao and H. Chen, "Small size NFC antenna with high performance," in *Proc. IEEE APS/URSI Int. Symp.*, Jun. 2016, pp. 1469–1470.
- [25] J.-Q. Zhu *et al.*, "A useful methodology to convert the smartphone metal cover into an antenna booster for NFC applications," *IEEE Trans. Antennas Propag.*, vol. 67, no. 7, pp. 4463–4473, Jul. 2019.
- [26] AN 11576PN548 *Antenna Design Guide*, NXP Semicond., Eindhoven, The Netherlands, Appl. Note, Rev. 0.5, Jun. 2015.
- [27] *IEEE Standard for Safety Levels with Respect to Human Exposure to Radio Frequency Electromagnetic Fields, 3 kHz to 300 GHz*, Standard C95.1 Edition-1999, 2005.
- [28] *International Electrotechnical Commission, Method of Measurement of Touch Current and Protective Conductor Current*, document IEC 60990, 1999.
- [29] J. Cho, J. Sun, H. Kim, J. Fan, Y. Lu, and S. Pan, "Coil design for 100 KHz and 6.78 MHz WPT system :Litz and solid wires and winding methods," in *Proc. IEEE Symp. Electromagn. Compat. Signal Integr.*, Washington, DC, USA, Aug. 2017, pp. 803–806.
- [30] *NFC Forum Tag Antenna Type*. Accessed: Dec. 13, 2019. [Online]. Available: <https://nfc-forum.org/our-work/specifications-and-application-documents/specifications/tag-type-technical-specifications/>
- [31] M.-A. Chung and C.-F. Yang, "Miniaturized NFC antenna design for a tablet PC with a narrow border and metal back-cover," *IEEE Antennas Wireless Propag. Lett.*, vol. 15, pp. 1470–1474, Dec. 2016.
- [32] C. Liu, A. P. Hu, G. A. Covic, and N.-K.-C. Nair, "Comparative study of CCPT systems with two different inductor tuning positions," *IEEE Trans. Power Electron.*, vol. 27, no. 1, pp. 294–306, Jan. 2012.
- [33] C. Liu, A. P. Hu, and X. Dai, "A contactless power transfer system with capacitively coupled matrix pad," in *Proc. IEEE Energy Convers. Congr. Exposit.*, Sep. 2011, pp. 3488–3494.
- [34] M. Kline, I. Izyumin, B. Boser, and S. Sanders, "Capacitive power transfer for contactless charging," in *Proc. IEEE 26th Annu. Appl. Power Electron. Conf. Expo.*, Mar. 2011, pp. 1398–1404.
- [35] D. C. Ludois, J. K. Reed, and K. Hanson, "Capacitive power transfer for rotor field current in synchronous machines," *IEEE Trans. Power Electron.*, vol. 27, no. 11, pp. 4638–4645, Nov. 2012.
- [36] C. Liu, A. P. Hu, and N. K. C. Nair, "Modelling and analysis of a capacitively coupled contactless power transfer system," *IET Power Electron.*, vol. 4, pp. 808–815, Aug. 2011.



**Jia-Qi Zhu** was born in Henan, China, in 1992. He received the B.S. degree in electronic information science and technology from Southwest Jiaotong University (SWJTU), Chengdu, China, in 2014. He is currently pursuing the Ph.D. degree with the University of Electronic Science and Technology of China (UESTC), Chengdu.

In 2018, he received funding from UESTC and China Scholarship Council and became a joint Ph.D. Student with the Department of Electrical and Computer Engineering, San Diego State University, San Diego, CA, USA. His main research interests are near-field communication (NFC) and wireless power transfer (WPT) antennas for smartphone applications, especially near-field antennas operating with metal-cover smartphones.



**Yong-Ling Ban** was born in Henan, China. He received the B.S. degree in mathematics from Shandong University, Jinan, China, in 2000, the M.S. degree in electromagnetics from Peking University, Beijing, China, in 2003, and the Ph.D. degree in microwave engineering from the University of Electronic Science and Technology of China (UESTC), Chengdu, China, in 2006.

In July of 2006, he joined the Xi'an Mechanical and Electric Information Institute, Xi'an, China, as a Microwave Engineer. He then joined Huawei Technologies Company Ltd., Shenzhen, China. At Huawei, he designed and implemented various terminal antennas for 15 data card and mobile phone products customized from leading telecommunication industries like Vodafone. From September 2010 to July 2016, he was an Associate Professor with UESTC, where he is currently a Professor. From May 2014 to April 2015, he visited the Queen Mary University of London, London, U.K., as a Scholar Visitor. His research interests include wideband small antennas for 4G/5G handset devices, multi-in multi-out (MIMO) antenna, and millimeter-wave antenna array. He has authored more than 60 referred journal and conference articles on these topics. He holds 20 granted and pending Chinese and overseas patents.



**Rui-Min Xu** (Member, IEEE) was born in Sichuan, China, in 1958. He received the B.S. and Ph.D. degrees in electromagnetic field and microwave techniques from the University of Electronic Science and Technology of China (UESTC), Chengdu, China, in 1982 and 2007, respectively.

He is currently a Full Professor with UESTC. His current research interests include microwave- and millimeter-wave technologies and applications, and radar systems.



**Chunting Chris Mi** (Fellow, IEEE) received the B.S.E.E. and M.S.E.E. degrees in electrical engineering from Northwestern Polytechnical University, Xi'an, China, and the Ph.D. degree in electrical engineering from the University of Toronto, Toronto, ON, Canada, in 1985, 1988, and 2001, respectively.

He was with the University of Michigan, Dearborn, Dearborn, MI, USA, from 2001 to 2015. He is currently a Professor and the Chair of electrical and computer engineering and the Director of the Department of Energy (DOE)—funded Graduate Automotive Technology Education (GATE) Center for Electric Drive Transportation, San Diego State University, San Diego, CA, USA.